Preliminary Studies for One-Step Fabrication of Metallic Iron-Based Coatings on Magnesium as Temporary Protection in Biodegradable Medical Application

Yuyun Yang[1,2,3], Zizhong Shi[1], Xiufang Cui[1]*, Yuejun Liu[1], Guo Jin[1], Sannakaisa Virtanen[3], Aldo R. Boccaccini[2] and Peng She[4]*

[1]Department of Material Science and Chemical Engineering, Institute of Surface/Interface Science and Technology, Harbin Engineering University, Harbin, China, [2]Department of Materials Science and Engineering, Institute of Biomaterials, University of Erlangen-Nuremberg, Erlangen, Germany, [3]Department of Materials Science and Engineering, Institute for Surface Science and Corrosion, University of Erlangen-Nuremberg, Erlangen, Germany, [4]Department of Orthopaedics, The Seventh Affiliated Hospital of Sun Yat-sen University, Shenzhen, China

Iron and magnesium are being considered as promising candidates for biodegradable materials in medical applications, both materials having their specific advantages and challenges. A hybrid of metallic iron and magnesium in a layered composite is studied in the present work, to combine the merits of both metals. A single-step dip-coating method was employed to prepare the layered composite material. Morphology, composition, crystal structure and corrosion behavior of the Mg/Fe sheet were assessed by SEM, EDX, XRD, and electrochemical measurements. The Mg/Fe layered composite sheet is composed of the magnesium substrate, a 1–2 μm metallic iron coating, and a pompon-like $Mg(OH)_2$/MgO top layer. Long-term open-circuit potential measurements revealed that the Mg/Fe sheet samples exhibit a "self-healing" effect in Dulbecco's modified Eagle's medium.

Keywords: iron, magnesium, one-step fabrication, composite, "self-healing" effect

1 INTRODUCTION

Since Lane introduced the application of metal plates for bone fracture fixation 100 years ago, metallic biomaterials have achieved huge development for a variety of biomedical applications (Hornberger et al., 2012; Mao et al., 2017; Li et al., 2019). The most well-known metallic biomaterials are high corrosion-resistant materials, such as 316 stainless steel (Tan et al., 2003; Shih et al., 2004; Patnaik et al., 2020), cobalt-chromium alloys (Ducheyne and Healy, 1988; Que and Topoleski, 2000; Kereiakes et al., 2003; Watanabe et al., 2021), titanium and its alloys (Helary et al., 2009; Huang et al., 2010; Niinomi et al., 2012; Jin et al., 2015; Lourenço et al., 2020), tantalum alloys (Miyazaki et al., 2000; Shimko et al., 2005; Zhou et al., 2007; Rodriguez-Contreras et al., 2021), as well as precious alloys (O'Brien, 1997; Chen et al., 2005; Niinomi et al., 2015). Another group of metals consists of biodegradable materials, such as pure iron and a variety of Fe-based alloys as well as pure magnesium and Mg alloys (Wu et al., 2016; Mao et al., 2017; Yang et al., 2018; Gorejová et al., 2019; Costantino et al., 2020; Zhu et al., 2021).

In the meantime, elements such as Fe and Mg are also considered as essential trace elements participating in a wide variety of metabolic processes, such as enzyme catalysis, oxygen transport,

energy metabolism, and DNA and RNA synthesis (Zhang et al., 2018; Lee et al., 2021). Released Fe and Mg ions during biodegradation reactions directly incorporate into the metabolic processes, affecting the metabolic functions and the biodegradation of metallic implants.

Compared with non-degradable materials, biodegradable metals should not cause permanent physical irritation and they avoid the need to remove a temporary implant in a second operation (Schinhammer et al., 2013; Mao et al., 2017). In principle, a controllable degradation rate should be achieved as this is a key requirement for degradable metallic biomaterials. Regarding degradation, Mg (Mg alloys) and Fe (Fe alloys) present different challenges. For example, the high dissolution rate of magnesium in biological environments largely limits its biomedical application (Fischerauer et al., 2013). Therefore, various surface modification and coating methods (Rajabalizadeh and Seifzadeh, 2014; Seifzadeh and Farhoudi, 2016; Nezamdoust et al., 2019; Abdi-Alghanab et al., 2020; Ouyang et al., 2020; Chen et al., 2021) are applied to tailor the undesired fast degradation rate into a moderate one to fulfill the therapeutic tasks. For instance, Zhu (Zhu et al., 2021) prepared a poly (d,l-lactic acid)-coated magnesium alloy-based rapamycin drug-eluting bioresorbable stent. *In vivo* and *in vitro* studies showed that the polymeric coatings provided a suitable degradation rate of magnesium alloy stents.

Compared with Mg-based alloys, pure iron and its alloys exhibit better mechanical properties and cause no excessive hydrogen evolution during degradation. On the contrary, several studies have been performed to increase the degradation rate of Fe-based materials for the possible application in temporary implants, as Fe-based materials show a too slow corrosion rate in biological environments (Abou Neel et al., 2005; Moravej et al., 2010; Zhang et al., 2010; Francis et al., 2015; Gorejová et al., 2019; Lee et al., 2021). For example in the research of Lee et al. (Lee et al., 2021) a novel combination of nanostructured surface topography and galvanic reaction was reported to achieve a uniform and accelerated degradation of a Fe implant.

Based on related research work on tailoring the degradation behavior of both biodegradable Mg materials (to decrease degradation) and Fe materials (to increase degradation), the idea of combining Mg and Fe together, especially by using iron coating as temporary protection of Mg substrates, is a feasible approach. In this design, two biocompatible metallic materials are introduced in one system, which greatly enhances the biocompatibility of the combined material for further investigation. On the other hand, the metallic iron serving as temporary protection on Mg would achieve the goal of tailoring the degradation rate of both Mg and Fe at the same time. Metallic iron coatings could protect magnesium substrates from aggressive corrosion attacks in the physiological environment until the metallic iron coatings are fully biodegraded. Meanwhile, by comparing with the degradation performance of bulk Fe materials, the degradation behavior of Fe coatings will be intensively affected by their thickness and structure.

Hence, in this study, metallic iron coatings are produced on magnesium substrates by a simple single-step dip-coating
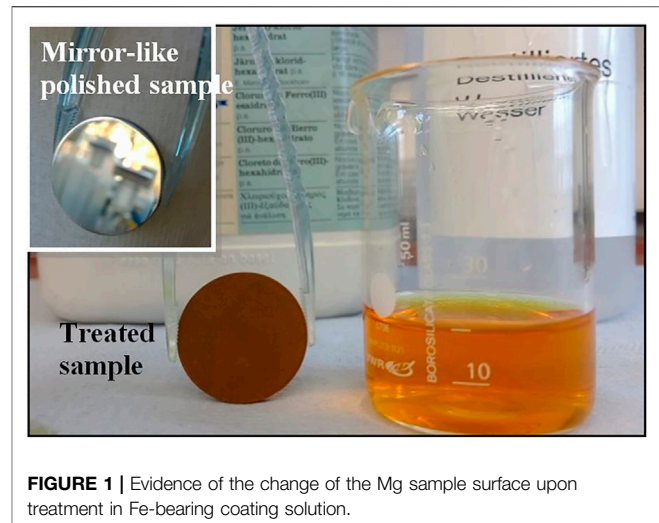
FIGURE 1 | Evidence of the change of the Mg sample surface upon treatment in Fe-bearing coating solution.

method. The reactions taking place in an aqueous solution are spontaneously driven by the electrochemical properties of the participating elements Mg and Fe, and no external energy was introduced during the process (Yan and Xue, 2006). This approach is in contrast to previous attempts to produce metallic coatings via several deposition ways, such as high velocity oxygen fuel, plasma spraying, physical vapor deposition, laser cladding, sol-gel, and kinetic spraying (Livsey, 1981; Liu et al., 2009; Nezamdoust and Seifzadeh, 2017; Dayani et al., 2018; Ferrández-Montero et al., 2019; Lin et al., 2021; Akhter et al., 2022). In most of these methods, fine powders as feedstock and a complex apparatus are needed to fabricate the metallic coatings on the substrate. The here explored one-step dip-coating method combines biodegradable metallic magnesium and iron together in one composite, and the different degradation behaviors of the two metals are exploited. The principle of the coating process is the immersion plating of Fe, taking advantage of the difference in the electrochemical potentials of the substrate and the coating material.

2 EXPERIMENTAL

2.1 Materials Preparation

Commercially pure magnesium rod of 25.4 mm diameter and 99.9% purity, (Chempur Feinchemikalien und Forschungsbedarf GmbH, Germany) was cut into 2–4 mm thickness slices to be used as substrates. A 1200 grit Microcut fleece (Buehler GmbH, Germany) was used for grinding with an ethanol/glycerol (3:1) mixture as lubricant. After that, the samples were cleaned in ultra-sonic bath in ethanol for 3 min. Subsequently, the samples were polished in three steps with diamond paste (6 μm, 3 μm, 1 μm) and a lubricant which consisted of distilled water/ethanol/neutral soap (1,000 ml:250 ml:10 g), followed by ultrasonic cleaning immediately after each polishing step. All samples were rinsed with ethanol and dried with hot air stream.

The fabrication of the layered composite coating was carried out by a dip-coating method. According to the electrochemical

series of the elements, a metal cation in an electrolyte can be reduced by any metal with a lower electrochemical potential. In this study, a less noble Mg substrate was applied to reduce Fe^{3+} into Fe and, as a consequence, Mg was oxidized into Mg^{2+} during the dipping process. The chemical reaction is according to **Eq. 1**.

$$3Mg + 2Fe^{3+} \rightarrow 3Mg^{2+} + 2Fe \qquad (1)$$
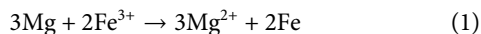
For this process, 1 g iron (III) chloride hexahydrate (Sigma-Aldrich) was completely dissolved in 20 ml de-ionized water under magnetic stirring for 5 min. The Mg substrates were immersed in the coating solution. The dip coating procedure was carried out at room temperature for 90 s. Immediately after being taken out from the suspension, the samples were rinsed in ethanol for 20 s and dried with hot air stream. As shown in **Figure 1**, mirror-like polished magnesium samples were completely covered by a brown composite coating after the treatment. A thin outer oxidized iron layer formed after taking the samples out from the suspension which could contribute to the brown color.

2.2 Microstructure and Composition of the Coatings

The surface and cross-section morphology and the chemical composition of the fabricated layered composite coatings were examined *via* a scanning electron microscope (SEM, model Auriga, Zeiss) equipped with energy-dispersive X-ray spectroscopy (EDX). The cross-sectional samples were prepared by Ar ion milling system (IM4000, HITACHI). X-ray diffraction (XRD) was performed using an X'pert Philips MPD instrument (equipped with Panalytical X'celerator detector, Germany) employing graphite monochromized Cu Kα radiation (Wavelength 1.54056 Å).

2.3 Electrochemical Measurements

Electrochemical behavior of the samples was investigated by using an electrochemical workstation "IM6eX" (Zahner-Elektrik GmbH and Co. KG, Kronach, Germany). Dulbecco's modified Eagle's medium (DMEM, Biochrome AG) was used as the electrolyte. The measurements were carried out in a conventional three-electrode cell assembly which consisted of the coated sample as the working electrode, a platinum plate as the auxiliary electrode and an Ag/AgCl electrode in 3-M KCl as the reference electrode. Long-term open-circuit potential (OCP) was monitored continuously up to 8 h in DMEM at room temperature. DMEM was refreshed every 8 h to mimic the physical buffering environment. To accelerate corrosoin, the samples were potentiodynamically polarized with sweep rate of 3 mV/s into the anodic direction.

3 RESULTS AND DISCUSSION

3.1 Microstructure and Composition

Morphology and elemental composition of freshly prepared samples were studied via SEM coupled with EDX and representative results are shown in **Figure 2**. EDX analysis was carried out on the whole surface and at special locations to determine the composition of the

layered composite coating. Clusters, as magnified in **Figure 2A**, precipitated randomly on the entire surface. These clusters were principally composed of metallic iron, such as at Spot 2 in **Figure 2B**. The iron signal indicates successful chemical conversion reaction, namely reduction of Fe^{3+} into Fe by the less noble Mg substrate (subsequent XRD results confirm this observation as discussed below). In the general survey 62.43 wt% iron was detected, with 25.73 wt% of O, 8.27 wt% of Mg, and 3.57 wt% of Cl. The small amount of chlorine is incorporated in the coating as a contamination from the reaction solution. The weight percentage of Mg at Spot 1 in **Figure 2A**, that is the rather flat area between the clusters, represents the highest value (12.34 wt%) compared with that of the whole area and that in Spot 2. In any case, the surface of the sample mostly consists of iron.

3.2 Crystal Structure of the Coatings

XRD measurements were conducted to characterize the crystal structure of the formed coatings. **Figure 3** shows the XRD patterns of pure Mg, pure Fe and the treated sample. All peaks in the pattern of the hybrid laminate appear in the exactly corresponding position to those of pure Mg and pure Fe substrates. Besides, a weak peak at approx. 60°, 2θ are assigned to $Mg(OH)_2$. XRD results therefore confirm that the layered composite coating is mainly composed of metallic Mg and Fe, and small amount of $Mg(OH)_2$, which is in good agreement with the EDX results.

The proposed formation mechanism of the particular structure shown in **Figure 2A** is schematically illustrated in **Figure 4**. The chemical reactions occurring during the dipping process are schematically shown to explain the mechanism. As Mg is less noble than Fe, metallic Fe can be formed on Mg from the Fe^{3+} ion containing solution. Therefore, upon immersion of pure Mg samples in $FeCl_3$ solution, the following chemical reactions take place:

$$3Mg + 2Fe^{3+} \rightarrow 2Fe + 3Mg^{2+}$$
$$Mg + 2H_2O \rightarrow Mg(OH)_2\downarrow + H_2\uparrow$$
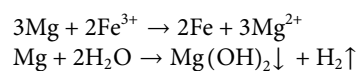
The sites of Fe^{3+} ion reduction and deposition as metallic Fe coincide with the sites of metallic Mg oxidation into Mg^{2+} and its dissolution. Simultaneously, with the hydrolysis of water, H_2 is produced and OH^- released. Mg^{2+} can easily precipitate with OH^- as $Mg(OH)_2$, hence depositing on the surface as well.

After 2 weeks storage in air, the surface morphology and chemical composition of the prepared samples were observed again by SEM coupled with EDX, as shown in **Figure 5**. Compared with the fresh sample, a characteristic "pompon-like" structure is formed at the sites between clusters, for instance near Spot 3 and framed areas in **Figure 5A**. The framed areas are shown in magnification to reveal the nano scale features on the surface, showing the presence of nano needles or nano wires branching out in all directions from the center of the pompon. EDX analysis revealed that the locations of the pompons are primarily enriched with Mg (35.89 wt%) and O (57.98 wt%), but contain only traces of Fe (0.1 wt%), such as in Spot 3. Conversely, much less Mg (4.61 wt%) and O (4.04 wt%) are detected in other areas, such as in Spot 5, where the random disorganized clusters are observed, while 84.43 wt% Fe is discovered in this spot. As regards the chemical composition in
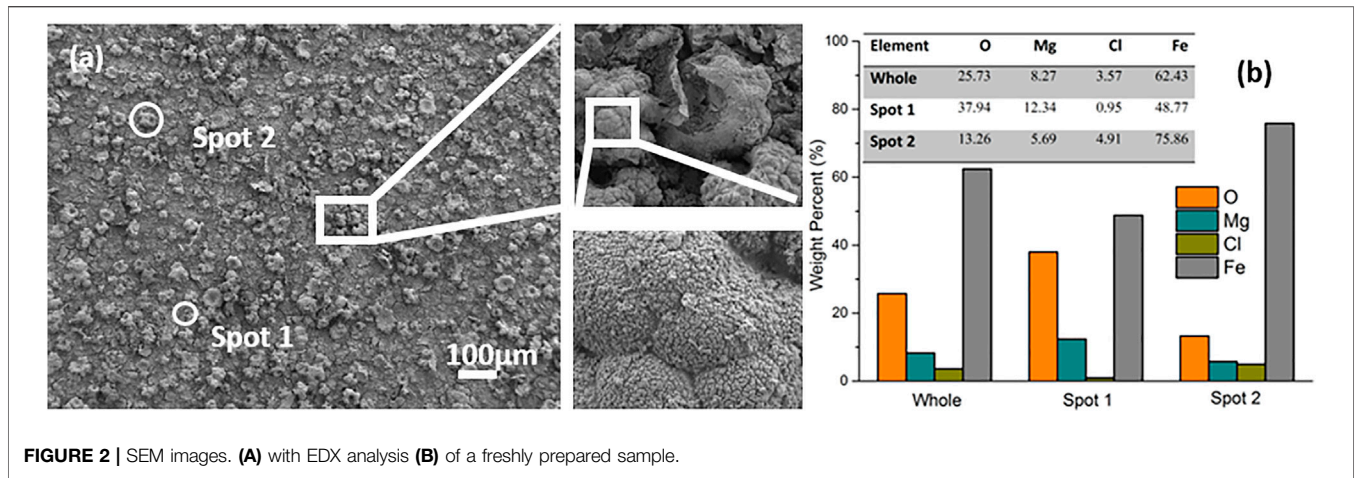
FIGURE 2 | SEM images. **(A)** with EDX analysis **(B)** of a freshly prepared sample.
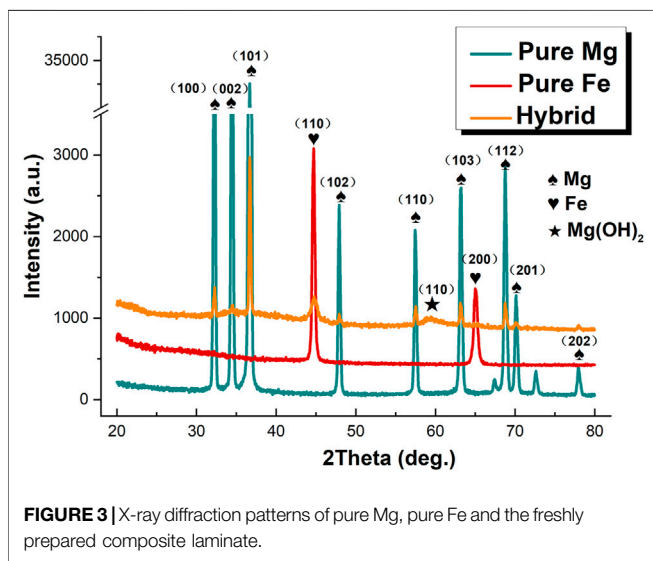
FIGURE 3 | X-ray diffraction patterns of pure Mg, pure Fe and the freshly prepared composite laminate.

increasing amounts of O and Mg on the whole surface, namely, from 25.73 wt% and 8.27 wt% in the fresh sample (in **Figure 2B**) up to 49.79 wt% and 37.32 wt% after lying in air (**Figure 5B**). Since Mg is more active than Fe under atmospheric conditions, galvanic corrosion has occurred between these two metals. As a result, Mg has been oxidized into pompon-like $MgO/Mg(OH)_2$ structures gradually forming on the whole surface, and metallic iron has remained unattacked. The process is schematically shown in **Figure 6**. Eventually, the resulting structure is a metallic Fe coating buried under a $Mg(OH)_2$ layer, as shown by the cross-sectional element mapping in **Figure 7**.

3.3 Cross-Section Morphology and Composition

For observing the morphology and element distribution from cross sections of the hybrid laminate after 2-week exposure to ambient air, SEM observations and EDX elemental mapping were carried out, as shown in **Figure 7**. The total thickness of the coating was determined to be approximately 19.4 μm. Elemental mapping of the cross-section revealed an uneven distribution of Mg, O, Fe, and Cl through the thickness of the coating. The top layer contains mainly Mg and O, this layer also shows cracks which are typical for $MgO/Mg(OH)_2$ surface layers. In addition,

Spot 4, the total weight percentage of Mg and O takes up more than 99% throughout the coating. In addition, many fine cracks are observed, which is a typical observation for conversion coatings on magnesium (Cui et al., 2012). Storage in air results in strongly
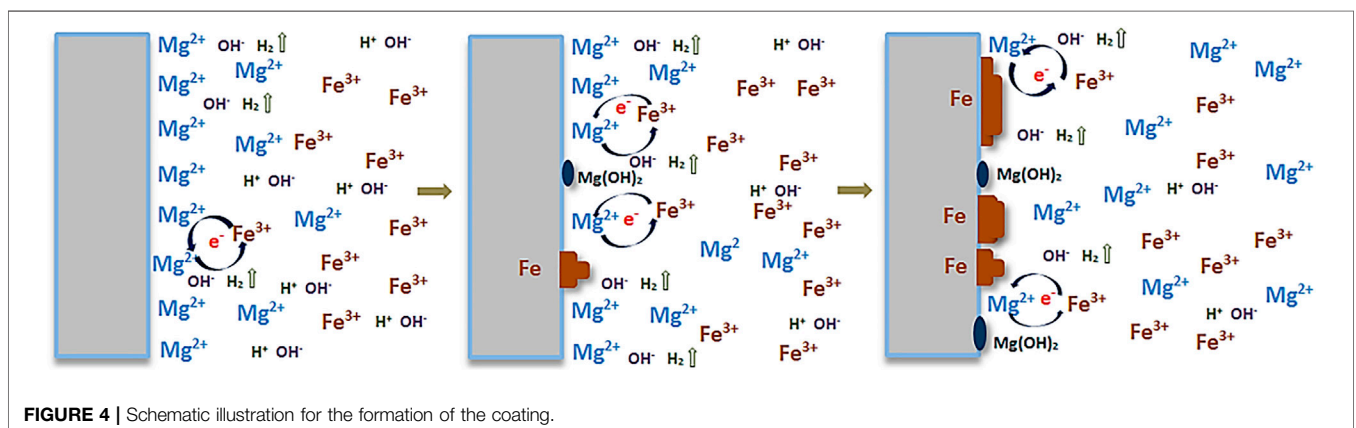
FIGURE 4 | Schematic illustration for the formation of the coating.
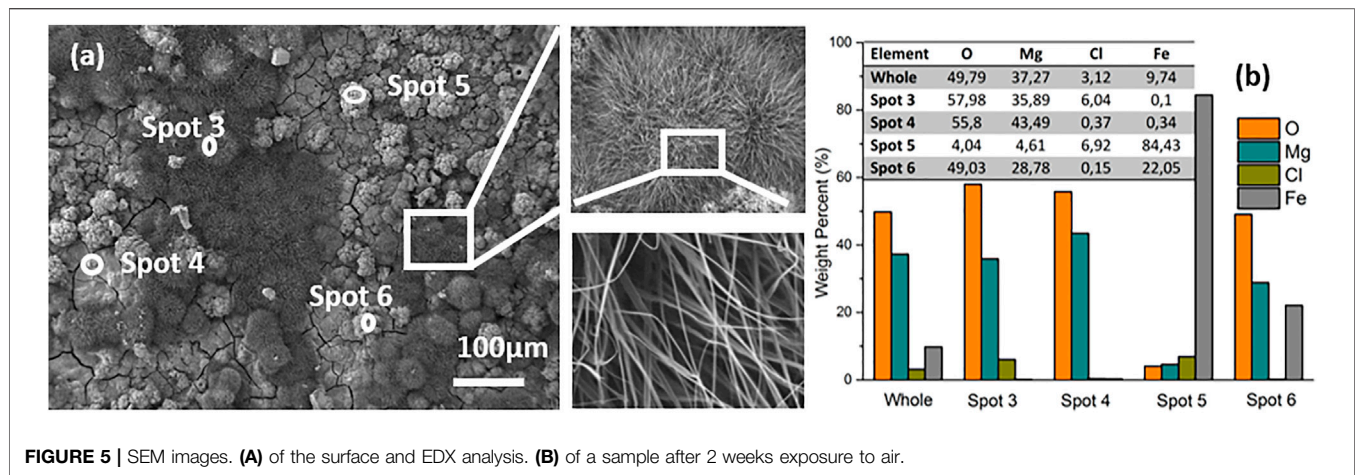
FIGURE 5 | SEM images. **(A)** of the surface and EDX analysis. **(B)** of a sample after 2 weeks exposure to air.
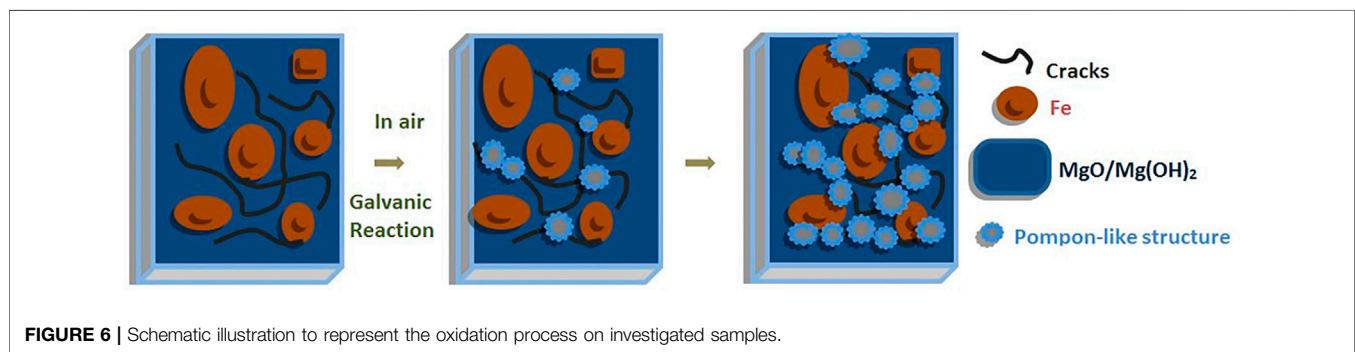
FIGURE 6 | Schematic illustration to represent the oxidation process on investigated samples.

the chlorine contamination is only present in the uppermost part of the surface layer. Interestingly, the Fe coating with a thickness of 1–2 μm is buried under the top $MgO/Mg(OH)_2$ layer, as suggested in the schematic diagram in **Figure 6**. Additional $MgO/Mg(OH)_2$ formation can be seen at sites of cracks through the top $MgO/Mg(OH)_2$ and the Fe layers.

3.4 Corrosion Behavior
3.4.1 OCP Measurements
To investigate the corrosion behavior of the new layered metals, long-term open-circuit potential (OCP) measurements were carried out in DMEM for the coated sample, as well as for pure Fe and pure Mg. The OCP variation as a function of time for the different samples is shown in **Figure 8**. Clearly, pure Mg and pure Fe samples reach a rather stable value around −1.75 V after 2500 s and −0.7 V after 4000 s, respectively, whereas the OCP of the coated sample fluctuated markedly between −0.2 V and −1.2 V during the first 8 h immersion time. However, interestingly, the OCP always recovered back to near −0.2 V every time after a sharp drop down to values close to −1.2 V. These oscillations in the OCP indicate breakdown events in the coating (sharp drop of OCP), followed by "self-healing" of the coating, for instance by precipitation of $Mg(OH)_2$ or other corrosion products blocking the sites of coating breakdown. Similar oscillations occurred again during the 27–35 h OCP observation, but the potential in this case recovers back to around -500mV and the fluctuation frequency is reduced

compared with that during the first 0–8 h of immersion. After 46 h immersion in DMEM, OCP dropped down to around -1200mV and stayed stable in the following 4 h.

The "self-healing" effect in OCP curves mainly embodies the "pulling up" of the dropped OCP values to a much higher OCP level. It can be speculated that the pulling-up and dropping-down processes shown in OCP curves are strongly linked to the initiating and hindering of the galvanic reactions which are non-continuously happening between the magnesium substrate and the iron coating in DMEM. In the first 8 h of OCP measurement, the upper level of OCP curves was maintained at around −0.2 V. This upper level of OCP values was even less negative than that of pure iron, which stayed at around −0.7 V after 8 h tests. The reason behind this unique phenomenon might be the existence of iron oxides and other depositions in DMEM precipitating on the surface of the magnesium substrate. Meanwhile, galvanic reactions would be initiated at the defect sites where the magnesium substrate was not fully coated by metallic iron coatings and the deposited products. At this stage, the OCP curve demonstrates a sharp drop-down to a lower level, which reflects the proceeding of galvanic reactions. The galvanic reaction products, mainly composed of $Mg(OH)_2$ and other hydrated and carbonated (Mg,Ca)-phosphate (Wagener and Virtanen, 2016) formed near the micro-crack sites, would separate the connection between the magnesium substrate and the iron coating in the medium and impeding the galvanic reaction process. The prevailed "OFF" mode of the galvanic reaction induces the "self-healing" effect in OCP curves and the

FIGURE 7 | SEM images and EDX mapping of the cross-section of the hybrid laminate after 2 weeks exposure to air.
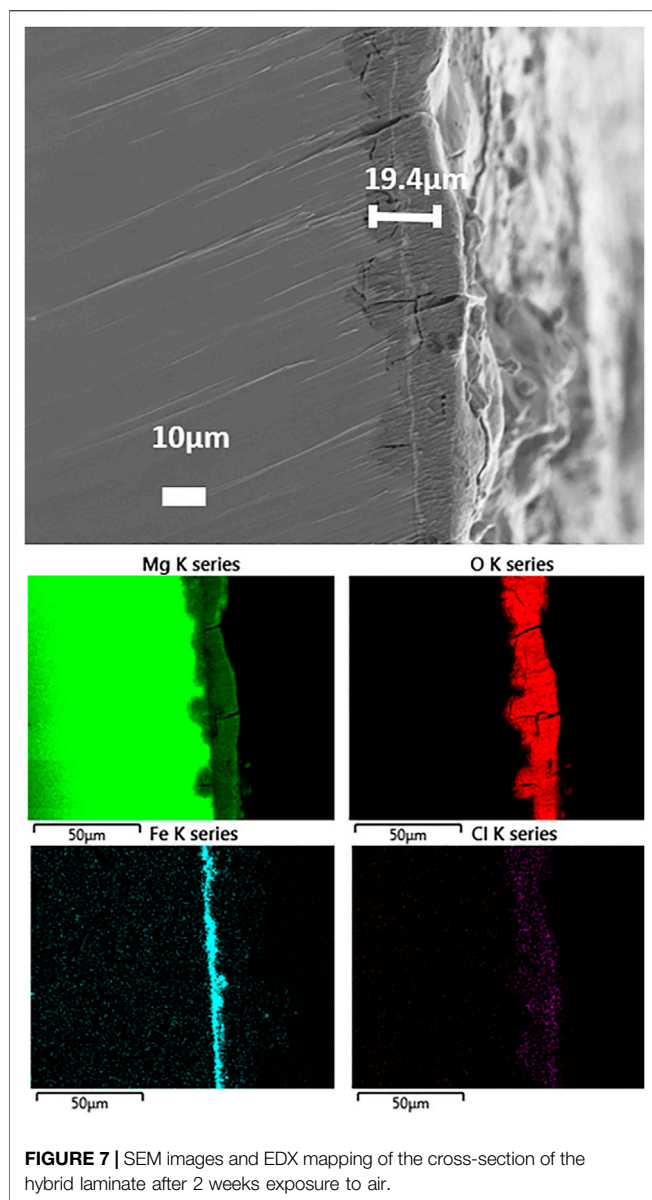
occasional "ON" mode of the galvanic reaction leads to the lower OCP level. The similar case can also be found in the curves of 27–35 h OCP, only the sharp potential dropping-down times and upper level of OCP decrease. The pH variation curve during the first 6 h of immersion and the potentiodynamic polarization curves of samples are displayed in the Supporting Information part.

In order to investigate changes in the morphology during the long-term OCP immersion experiment, samples were observed after 8 h (in **Figures 9A,B**) and 50 h (in **Figures 9C,D**) OCP monitoring in DMEM. As shown in **Figure 9A**, randomly distributed clusters are still displayed on the whole surface after 8 h OCP measurement. In the magnified images, many precipitates deposited on the surface can be observed. A typical magnesium conversion coating morphology with cracks is observed after 50 h OCP monitoring in **Figure 9C**. Protuberances, such as in Spot 11, could be seen on the separated pieces of the cracked coating in high magnification images in

Figure 9C. The results in **Figure 9B,D** show the coating composition in overview for the whole surface and for three different sites. Since the depositions formed on the top surface, EDX data in **Figures 9B,D** shows a nearly 50% reduced iron signals as compared with a fresh sample (in **Figure 2B**). On the other hand, the O content increased significantly from 25.73 wt% in **Figure 2B** to about 50 wt% in **Figures 9B,D**. With longer immersion time in DMEM, the weight percentage of Mg increased from ca. 10 wt % at 8 h up to 30 wt% at 50 h. The growing amount of O and Mg coincides with the formation of the typical cracked coating, as observed in **Figure 9C**.

Compounds containing Na, P, K, and Ca are incorporated in the surface layer and stem from the DMEM solution, which was employed as electrolyte for the OCP measurements. Overall, the levels of Na, P, K and Ca decrease from the values at 8 h in **Figure 9B** to the values at 50 h in **Figure 9D**. The decreasing trend might be due to the fact that the compounds containing such elements are buried by the subsequently formed $Mg(OH)_2$ on top.

3.4.2 Micromorphology and Composition After Electrochemical Measurements

To demonstrate the coating behavior under a highly accelerated corrosion scenario, the coated samples were polarized up to +1 V (this condition does not correspond to a normal corrosion scenario of Mg alloys, but the experiment was carried out to indicate a worst-case behavior). Corrosion products after the electrochemical measurement were examined by SEM along with EDX to determine the morphology and chemical composition. As shown in **Figure 10A**, the coating is still present on the surface, exhibiting some large clusters of compact precipitates. The tiny cracks spread between or through the clusters on the rough surface. The chemical composition of the corrosion products was analyzed by EDX. The results in **Figure 10** 2) show the composition in overview for the whole surface and for three different sites. For the overview, strong signals for Fe (54.53 wt%) and O (34.17 wt%) are observed, with some Ca (5.17%) and minor amounts of Mg, Na, Cl, P and K (in total 5 wt%). A similar case for element distribution is found at Spot 13 and Spot 14 in **Figure 10B**. The Fe content in Spot 12 (73.69 wt%)

FIGURE 8 | Open-circuit potential as a function of immersion time in DMEM.
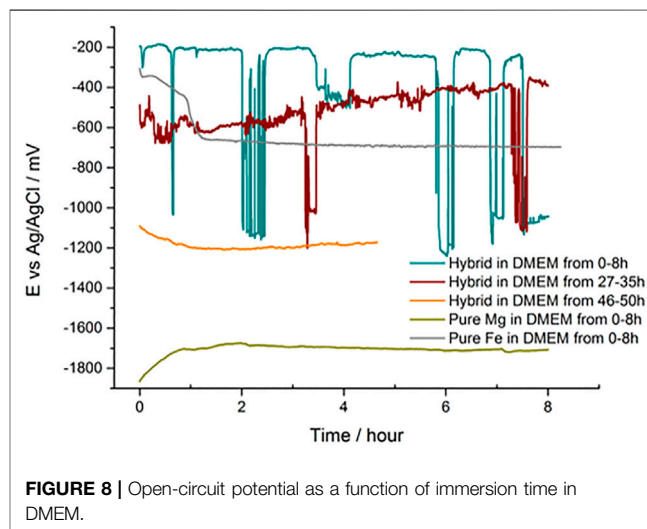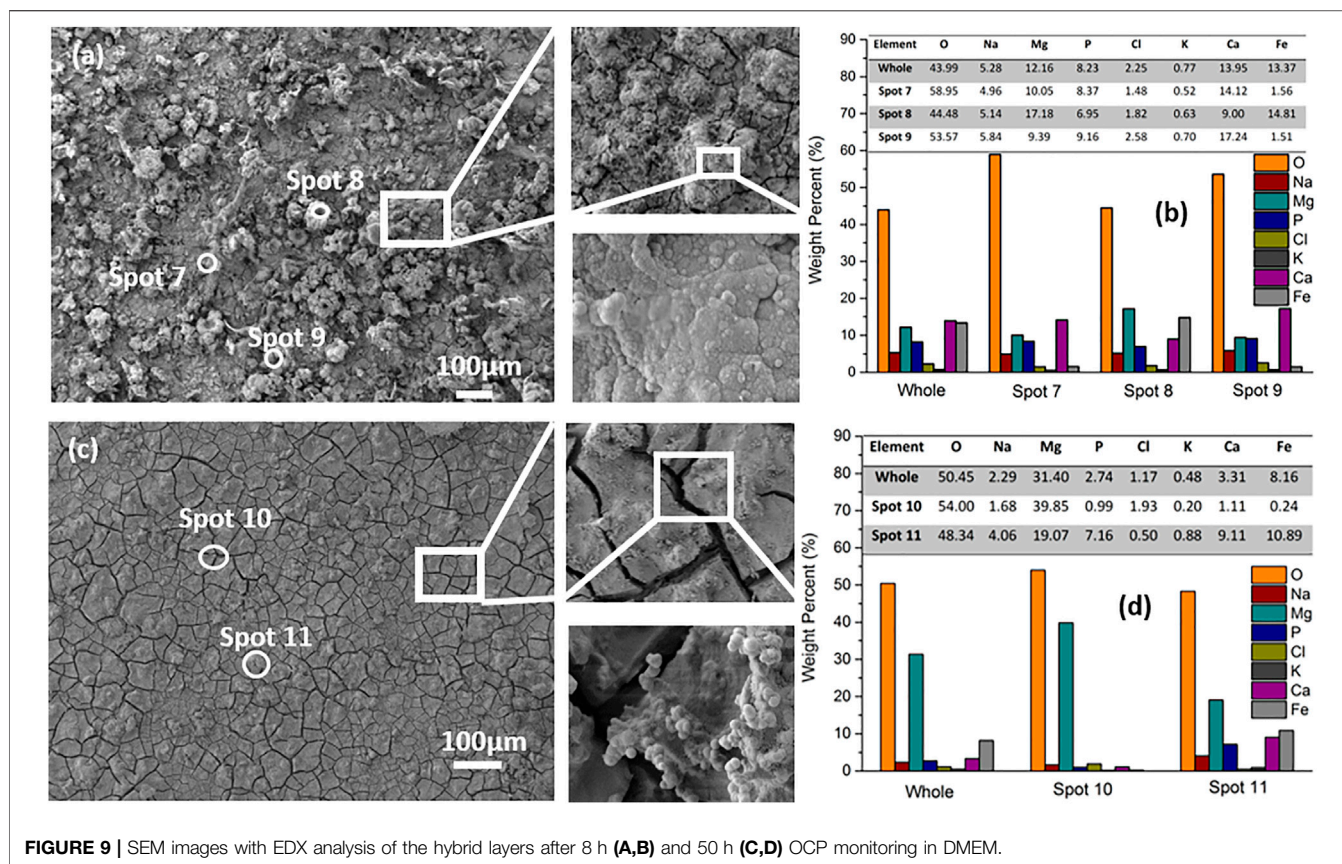
FIGURE 9 | SEM images with EDX analysis of the hybrid layers after 8 h (A,B) and 50 h (C,D) OCP monitoring in DMEM.
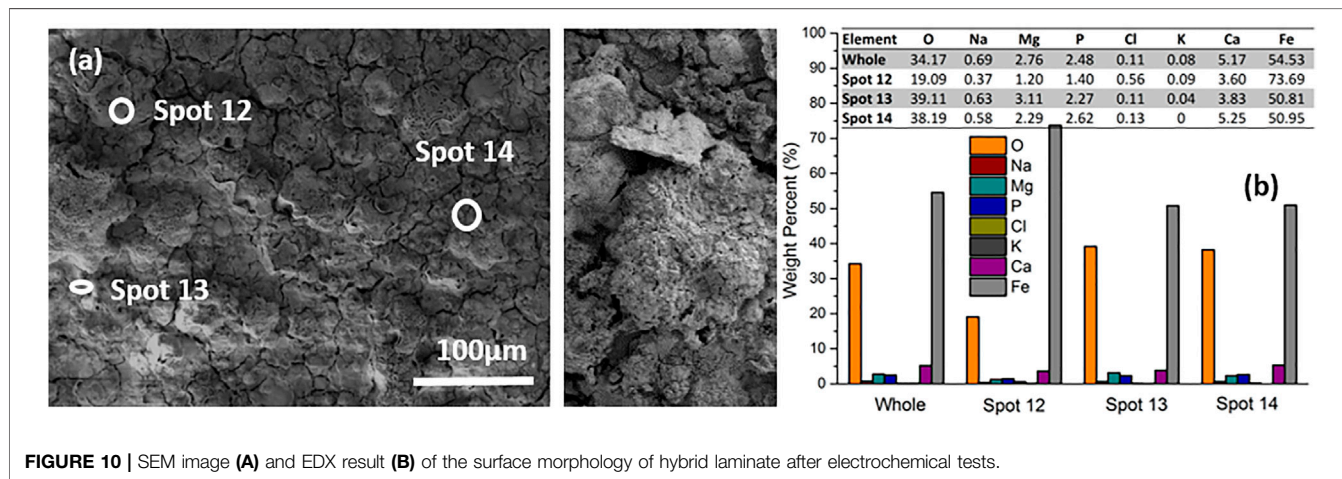
FIGURE 10 | SEM image (A) and EDX result (B) of the surface morphology of hybrid laminate after electrochemical tests.

is even higher than in the whole surface. The comparable presence of Fe and the significant decreased Mg content after the electrochemical measurement as compared with the average amount present in the fresh treated samples (see **Figure 2B**) may be attributed to the unstable MgO or $Mg(OH)_2$ and other components in the top layer that have dissolved during the testing period in DMEM, exposing the underlying Fe compact coating, as shown in **Figure 10A**. Noteworthy is that the Fe coating has not been destroyed by polarization up to + 1 V in DMEM. The Fe coating will work as a barrier against the penetration of external corrosive ions onto the

magnesium substrate. Furthermore, the weight percentage ratio of oxygen to iron in the fresh sample (**Figure 2**) and after electrochemical tests (**Figure 10**) increases approximately from 1: 3 to 1:2, revealing partial oxidation of the metallic iron.

4 CONCLUSION AND OUTLOOK

A simple, single-step dip coating process was used to fabricate a layered composite coating composed of metallic Fe and $Mg(OH)_2$

on a Mg substrate. A metallic Fe coating with a thickness of 1–2 μm is formed between the Mg substrate and a $Mg(OH)_2$/MgO top layer. Under immersion conditions in DMEM, the open-circuit potential of the coated samples shows large oscillations, indicating local breakdown events followed by a self-healing behavior of the coated samples.

The simple coating process developed here; based on spontaneous electrochemical reactions, combined with the self-healing nature of the composite coating, represent a promising approach for tackling the challenge of controlling the corrosion rate of both Mg and Fe. Further research will focus on attempting to increase the thickness of the coatings and decrease the presence of cracks in the coatings, as well as on further elucidation of the degradation mechanisms and the origin of the self-healing property of the coatings.

DATA AVAILABILITY STATEMENT

The original contributions presented in the study are included in the article/**Supplementary Material**, further inquiries can be directed to the corresponding author.

AUTHOR CONTRIBUTIONS

YY, SV, and AB have substantial contributions to the conception and design of the work. YY collected, analyzed, and interpretation of data for the work. XC, GJ, and PS organized the structure of the manuscript. ZS and YL were responsible for the experiments of pH variation and potentiodynamic polarization during the revision period. All authors contributed to manuscript revision, read, and approved the submitted version.

FUNDING

ACKNOWLEDGMENTS

SUPPLEMENTARY MATERIAL

The Supplementary Material for this article can be found online at: https://www.frontiersin.org/articles/10.3389/fmats.2021.786650/full#supplementary-material

REFERENCES

Abdi-Alghanab, K., Seifzadeh, D., Rajabalizadeh, Z., and Habibi-Yangjeh, A. (2020). High Corrosion Protection Performance of the LDH/Ni-P Composite Coating on AM60B Magnesium Alloy. *Surf. Coat. Technol.* 397, 125979. doi:10.1016/j.surfcoat.2020.125979

Abou Neel, E. a., Ahmed, I., Blaker, J. J., Bismarck, a., Boccaccini, a. R., Lewis, M. P., et al. (2005). Effect of Iron on the Surface, Degradation and Ion Release Properties of Phosphate-Based Glass Fibres. *Acta Biomater.* 1 (5), 553–563. doi:10.1016/j.actbio.2005.05.001

Akhter, R., Bendavid, A., and Munroe, P. (2022). Effect of Ni Content on the Microstructure and Mechanical Properties of TiNiN Coatings. *Appl. Surf. Sci.* 573, 151536. doi:10.1016/j.apsusc.2021.151536

Chen, J., Wiley, B., Li, Z.-Y., Campbell, D., Saeki, F., Cang, H., et al. (2005). Gold Nanocages: Engineering Their Structure for Biomedical Applications. *Adv. Mater.* 17 (18), 2255–2261. doi:10.1002/adma.200500833View/save

Chen, Y., Wu, L., Yao, W., Zhong, Z., Chen, Y., Wu, J., et al. (2021). One-Step *In Situ* Synthesis of Graphene Oxide/MgAl-Layered Double Hydroxide Coating on a Micro-arc Oxidation Coating for Enhanced Corrosion Protection of Magnesium Alloys. *Surf. Coat. Technol.* 413, 127083. doi:10.1016/j.surfcoat.2021.127083

Costantino, M. D., Schuster, A., Helmholz, H., Meyer-Rachner, A., Willumeit-Römer, R., and Luthringer-Feyerabend, B. J. C. (2020). Inflammatory Response to Magnesium-Based Biodegradable Implant Materials. *Acta Biomater.* 101, 598–608. doi:10.1016/j.actbio.2019.10.014

Cui, X., Jin, G., Yang, Y., Liu, E., Lin, L., and Zhong, J. (2012). The Formation of Neodymium Conversion Coating and the Influence of Post-Treatment. *Appl. Surf. Sci.* 258 (7), 3249–3254. doi:10.1016/j.apsusc.2011.11.073

Dayani, S. B., Shaha, S. K., Ghelichi, R., Wang, J. F., and Jahed, H. (2018). The Impact of AA7075 Cold Spray Coating on the Fatigue Life of AZ31B Cast Alloy. *Surf. Coat. Technol.* 337, 150–158. doi:10.1016/J.SURFCOAT.2018.01.008

Ducheyne, P., and Healy, K. E. (1988). The Effect of Plasma-Sprayed Calcium Phosphate Ceramic Coatings on the Metal Ion Release from Porous Titanium and Cobalt-Chromium Alloys. *J. Biomed. Mater. Res.* 22 (12), 1137–1163. doi:10.1002/jbm.820221207

Ferrández-Montero, A., Lieblich, M., González-Carrasco, J. L., Benavente, R., Lorenzo, V., Detsch, R., et al. (2019). Development of Biocompatible and Fully Bioabsorbable PLA/Mg Films for Tissue Regeneration Applications. *Acta Biomater.* 98, 114–124. doi:10.1016/J.ACTBIO.2019.05.026

Fischerauer, S. F., Kraus, T., Wu, X., Tangl, S., Sorantin, E., Hänzi, a. C., et al. (2013). *In Vivo* Degradation Performance of Micro-arc-oxidized Magnesium Implants: A Micro-CT Study in Rats. *Acta Biomater.* 9 (2), 5411–5420. doi:10.1016/j.actbio.2012.09.017

Francis, A., Yang, Y., Virtanen, S., and Boccaccini, A. R. (2015). Iron and Iron-Based Alloys for Temporary Cardiovascular Applications. *J. Mater. Sci. Mater. Med.* 26, 138. doi:10.1007/s10856-015-5473-8

Gorejová, R., Haverová, L., Oriňaková, R., Oriňak, A., and Oriňak, M. (2019). Recent Advancements in Fe-Based Biodegradable Materials for Bone Repair. *J. Mater. Sci.* 54 (3), 1913–1947. doi:10.1007/s10853-018-3011-z

Helary, G., Noirclere, F., Mayingi, J., and Migonney, V. (2009). A New Approach to Graft Bioactive Polymer on Titanium Implants: Improvement of MG 63 Cell Differentiation onto This Coating. *Acta Biomater.* 5 (1), 124–133. doi:10.1016/j.actbio.2008.07.037

Hornberger, H., Virtanen, S., and Boccaccini, A. R. (2012). Biomedical Coatings on Magnesium Alloys - A Review. *Acta Biomater.* 8 (7), 2442–2455. doi:10.1016/j.actbio.2012.04.012

Huang, H.-L., Chang, Y.-Y., Lai, M.-C., Lin, C.-R., Lai, C.-H., and Shieh, T.-M. (2010). Antibacterial TaN-Ag Coatings on Titanium Dental Implants. *Surf. Coat. Technology* 205 (5), 1636–1641. doi:10.1016/j.surfcoat.2010.07.096

Jin, G., Qin, H., Cao, H., Qiao, Y., Zhao, Y., Peng, X., et al. (2015). Zn/Ag Micro-galvanic Couples Formed on Titanium and Osseointegration Effects in the Presence of S. Aureus. *Biomaterials* 65, 22–31. doi:10.1016/j.biomaterials.2015.06.040

Kereiakes, D. J., Cox, D. A., Hermiller, J. B., Midei, M. G., Bachinsky, W. B., Nukta, E. D., et al. (2003). Usefulness of a Cobalt Chromium Coronary Stent Alloy. *Am. J. Cardiol.* 92 (4), 463–466. doi:10.1016/S0002-9149(03)00669-6

Lee, M. K., Lee, H., Park, C., Kang, I. G., Kim, J., Kim, H. E., et al. (2021). Accelerated Biodegradation of Iron-Based Implants via Tantalum-Implanted Surface Nanostructures. *Bioact. Mater.* 9, 239–250. doi:10.1016/j.bioactmat.2021.07.003

Li, C., Guo, C., Fitzpatrick, V., Ibrahim, A., Zwierstra, M. J., Hanna, P., et al. (2019). Design of Biodegradable, Implantable Devices towards Clinical Translation. *Nat. Rev. Mater.* 5, 61–81. doi:10.1038/s41578-019-0150-z

Lin, T. J., Sheu, H. H., Lee, C. Y., and Lee, H. Bin. (2021). The Study of Mechanical Properties and Corrosion Behavior of the Fe-Based Amorphous Alloy Coatings Using High Velocity Oxygen Fuel Spraying. *J. Alloys Compd.* 867, 159132. doi:10.1016/j.jallcom.2021.159132

Liu, X. Q., Zheng, Y. G., Chang, X. C., Hou, W. L., Wang, J. Q., Tang, Z., et al. (2009). Microstructure and Properties of Fe-Based Amorphous Metallic Coating Produced by High Velocity Axial Plasma Spraying. *J. Alloys Compd.* 484 (1–2), 300–307. doi:10.1016/j.jallcom.2009.04.086

Livsey, C. (1981). Apparatus for Application of Metallic Coatings to Metallic Substrates. *Patent* 4, 300.474.

Lourenço, M. L., Cardoso, G. C., Sousa, K. d. S. J., Donato, T. A. G., Pontes, F. M. L., and Grandini, C. R. (2020). Development of Novel Ti-Mo-Mn Alloys for Biomedical Applications. *Sci. Rep.* 10 (1), 1–8. doi:10.1038/s41598-020-62865-4

Mao, L., shen, L., Chen, J., Zhang, X., Kwak, M., Wu, Y., et al. (2017). A Promising Biodegradable Magnesium Alloy Suitable for Clinical Vascular Stent Application. *Sci. Rep.* 7 (1), 46343. doi:10.1038/srep46343

Miyazaki, T., Kim, H.-M., Miyaji, F., Kokubo, T., Kato, H., and Nakamura, T. (2000). Bioactive Tantalum Metal Prepared by NaOH Treatment. *J. Biomed. Mater. Res.* 50 (1), 35–42. doi:10.1002/(sici)1097-4636(200004)50:1<35::aid-jbm6>3.0.co;2-8

M. Niinomi, T. Narushima, and M. Nakai (Editors) (2015). *Advances in Metallic Biomaterials; Springer Series in Biomaterials Science and Engineering* (New York, United States: Springer). doi:10.1007/978-3-662-46842-5

Moravej, M., Purnama, a., Fiset, M., Couet, J., and Mantovani, D. (2010). Electroformed Pure Iron as a New Biomaterial for Degradable Stents: *In Vitro* Degradation and Preliminary Cell Viability Studies. *Acta Biomater.* 6 (5), 1843–1851. doi:10.1016/j.actbio.2010.01.008

Nezamdoust, S., and Seifzadeh, D. (2017). Application of CeH–V/Sol–Gel Composite Coating for Corrosion Protection of AM60B Magnesium Alloy. *Trans. Nonferrous Met. Soc. China (English Ed.)* 27 (2), 352–362. doi:10.1016/S1003-6326(17)60039-6

Nezamdoust, S., Seifzadeh, D., and Rajabalizadeh, Z. (2019). Application of Novel Sol–Gel Composites on Magnesium Alloy. *J. Magnes. Alloy.* 7 (3), 419–432. doi:10.1016/j.jma.2019.03.004

Niinomi, M., Nakai, M., and Hieda, J. (2012). Development of New Metallic Alloys for Biomedical Applications. *Acta Biomater.* 8 (11), 3888–3903. doi:10.1016/j.actbio.2012.06.037

O'Brien, W. (1997). *Dental Materials and Their Selection*. Chicago: Quintessence.

Ouyang, Y., Li, L. X., Xie, Z. H., Tang, L., Wang, F., and Zhong, C. J. (2020). A Self-Healing Coating Based on Facile PH-Responsive Nanocontainers for Corrosion Protection of Magnesium Alloy. *J. Magnes. Alloy.* doi:10.1016/j.jma.2020.11.007

Patnaik, L., Ranjan Maity, S., and Kumar, S. (2020). Status of Nickel Free Stainless Steel in Biomedical Field: A Review of Last 10 Years and What Else Can Be Done. *Mater. Today Proc.* 26, 638–643. doi:10.1016/j.matpr.2019.12.205

Que, L., and Topoleski, L. D. T. (2000). Third-Body Wear of Cobalt-Chromium-Molybdenum Implant Alloys Initiated by Bone and Poly(Methyl Methacrylate) Particles. *J. Biomed. Mater. Res.* 50 (3), 322–330. doi:10.1002/(sici)1097-4636(20000605)50:3<322::aid-jbm5>3.0.co;2-u

Rajabalizadeh, Z., and Seifzadeh, D. (2014). The Effect of Copper Ion on Microstructure, Plating Rate and Anticorrosive Performance of Electroless Ni-P Coating on AZ61 Magnesium Alloy. *Prot. Met. Phys. Chem. Surf.* 50 (4), 516–523. doi:10.1134/S2070205114040157

Rodriguez-Contreras, A., Moruno, C. M., Fernandez-Fairen, M., Rupérez, E., Gil, F. J., and Manero, J. M. (2021). "Other Metallic Alloys: Tantalum-Based Materials for Biomedical Applications," in *Structural Biomaterials* (Amsterdam, Netherlands: Elsevier), 229–273. doi:10.1016/b978-0-12-818831-6.00007-0

Schinhammer, M., Steiger, P., Moszner, F., Löffler, J. F., and Uggowitzer, P. J. (2013). Degradation Performance of Biodegradable Fe-Mn-C(-Pd) Alloys. *Mater. Sci. Eng. C. Mater. Biol. Appl.* 33 (4), 1882–1893. doi:10.1016/j.msec.2012.10.013

Seifzadeh, D., and Farhoudi, L. (2016). Electroless Co-P Plating on Magnesium Alloy and its Anti-corrosion Properties. *Surf. Eng.* 32 (5), 348–355. doi:10.1179/1743294415Y.0000000034

Shih, C.-C., Shih, C.-M., Su, Y.-Y., Su, L. H. J., Chang, M.-S., and Lin, S.-J. (2004). Effect of Surface Oxide Properties on Corrosion Resistance of 316L Stainless Steel for Biomedical Applications. *Corrosion Sci.* 46 (2), 427–441. doi:10.1016/S0010-938X(03)00148-3

Shimko, D. A., Shimko, V. F., Sander, E. A., Dickson, K. F., and Nauman, E. A. (2005). Effect of Porosity on the Fluid Flow Characteristics and Mechanical Properties of Tantalum Scaffolds. *J. Biomed. Mater. Res.* 73B (2), 315–324. doi:10.1002/jbm.b.30229

Tan, Q., Ji, J., Barbosa, M. A., Fonseca, C., and Shen, J. (2003). Constructing Thromboresistant Surface on Biomedical Stainless Steel via Layer-By-Layer Deposition Anticoagulant. *Biomaterials* 24 (25), 4699–4705. doi:10.1016/S0142-9612(03)00363-6

Wagener, V., and Virtanen, S. (2016). Protective Layer Formation on Magnesium in Cell Culture Medium. *Mater. Sci. Eng. C* 63, 341–351. doi:10.1016/j.msec.2016.03.003

Watanabe, K., Fukuzaki, S., Sugino, A., Benson, N., Metcalf, N., Nakamura, M., et al. (2021). Cobalt-Chromium Alloy Has Superior Antibacterial Effect Than Titanium Alloy. *Spine (Phila. Pa. 1976)* 46 (17), E911–E915. doi:10.1097/BRS.0000000000003970

Wu, Y., He, G., Zhang, Y., Liu, Y., Li, M., Wang, X., et al. (2016). Unique Antitumor Property of the Mg-Ca-Sr Alloys with Addition of Zn. *Nat. Publ. Gr.* 6, 21736. doi:10.1038/srep21736

Yan, C., and Xue, D. (2006). General, Spontaneous Ion Replacement Reaction for the Synthesis of Micro- and Nanostructured Metal Oxides. *J. Phys. Chem. B* 110 (4), 1581–1586. doi:10.1021/jp056373+

Yang, Y., Zhou, J., Detsch, R., Virtanen, S., Taccardi, N., Heise, S., et al. (2018). Biodegradable Nanostructures: Degradation Process and Biocompatibility of Iron Oxide Nanostructured Arrays. *Mater. Sci. Eng. C* 85 (October 2017), 203–213. doi:10.1016/j.msec.2017.12.021

Zhang, C., Lin, J., and Liu, H. (2018). Magnesium-Based Biodegradable Materials for Biomedical Applications. *MRS Adv.* 3 (40), 2359–2364. doi:10.1557/adv.2018.488

Zhang, E., Chen, H., and Shen, F. (2010). Biocorrosion Properties and Blood and Cell Compatibility of Pure Iron as a Biodegradable Biomaterial. *J. Mater. Sci. Mater. Med.* 21 (7), 2151–2163. doi:10.1007/s10856-010-4070-0

Zhou, Y.-L., Niinomi, M., Akahori, T., Nakai, M., and Fukui, H. (2007). Comparison of Various Properties between Titanium-Tantalum Alloy and Pure Titanium for Biomedical Applications. *Mater. Trans.* 48 (3), 380–384. doi:10.2320/matertrans.48.380

Zhu, J., Zhang, X., Niu, J., Shi, Y., Zhu, Z., Dai, D., et al. (2021). Biosafety and Efficacy Evaluation of a Biodegradable Magnesium-Based Drug-Eluting Stent in Porcine Coronary Artery. *Sci. Rep.* 11 (1), 1–12. doi:10.1038/s41598-021-86803-0